Measuring non-radiative relaxation time of fluorophores with biomedical applications by intensity-modulated laser-induced photoacoustic effect

Behrouz Soroushian and Xinmai Yang*

Bioengineering Research Center, Department of Mechanical Engineering, 5109 Learned Hall, 1530 West 15th Street, Lawrence, KS 66045, USA
**xmyang@ku.edu*

Abstract: Modulated tone-burst light was employed to measure non-radiative relaxation time of fluorophores with biomedical importance through photoacoustic effect. Non-radiative relaxation time was estimated through the frequency dependence of photoacoustic signal amplitude. Experiments were performed on solutions of new indocyanine green (IR-820), which is a near infrared dye and has biomedical applications, in two different solvents (water and dimethyl sulfoxide (DMSO)). A 1.5 times slower non-radiative relaxation for the solution of dye in DMSO was observed comparing with the aqueous solution. This result agrees well with general finding that non-radiative relaxation of molecules in triplet state depends on viscosity of solvents in which they are dissolved. Measurements of the non-radiative relaxation time can be used as a new source of contrast mechanism in photoacoustic imaging technique. The proposed method has potential applications such as imaging tissue oxygenation and mapping of other chemophysical differences in microenvironment of exogenous biomarkers.

OCIS codes: (110.5125) Photoacoustics; (170.6510) Spectroscopy, tissue diagnostics; (300.6380) Spectroscopy, modulation

References and links

1. M. Y. Berezin and S. Achilefu, "Fluorescence lifetime measurements and biological imaging," Chem. Rev. **110**(5), 2641–2684 (2010).
2. Y. H. Sun, N. Hatami, M. Yee, J. Phipps, D. S. Elson, F. Gorin, R. J. Schrot, and L. Marcu, "Fluorescence lifetime imaging microscopy for brain tumor image-guided surgery," J. Biomed. Opt. **15**(5), 056022 (2010).
3. J.-M. I. Maarek, L. Marcu, M. C. Fishbein, and W. S. Grundfest, "Time-resolved fluorescence of human aortic wall: use for improved identification of atherosclerotic lesions," Lasers Surg. Med. **27**(3), 241–254 (2000).
4. P. H. Carpentier, "Méthodes actuelles d'exploration clinique de la microcirculation," J. Mal. Vasc. **26**(2), 142–147 (2001).
5. S. Murata, P. Herman, H. J. Lin, and J. R. Lakowicz, "Fluorescence lifetime imaging of nuclear DNA: effect of fluorescence resonance energy transfer," Cytometry **41**(3), 178–185 (2000).
6. A. Danielli, C. P. Favazza, K. Maslov, and L. V. Wang, "Single-wavelength functional photoacoustic microscopy in biological tissue," Opt. Lett. **36**(5), 769–771 (2011).
7. A. Danielli, C. P. Favazza, K. Maslov, and L. V. Wang, "Picosecond absorption relaxation measured with nanosecond laser photoacoustics," Appl. Phys. Lett. **97**(16), 163701 (2010).
8. S. Ashkenazi, S. W. Huang, T. Horvath, Y. E. L. Koo, and R. Kopelman, "Photoacoustic probing of fluorophore excited state lifetime with application to oxygen sensing," J. Biomed. Opt. **13**(3), 034023 (2008).
9. K. Maslov and L. V. Wang, "Photoacoustic imaging of biological tissue with intensity-modulated continuous-wave laser," J. Biomed. Opt. **13**(2), 024006 (2008).
10. Y. Fan, A. Mandelis, G. Spirou, and I. A. Vitkin, "Development of a laser photothermoacoustic frequency-swept system for subsurface imaging: theory and experiment," J. Acoust. Soc. Am. **116**(6), 3523–3533 (2004).
11. M. Ouzafe, P. Poulet, and J. Chambron, "Photoacoustic detection of triplet state and singlet oxygen in highly absorbing samples," Photochem. Photobiol. **55**(4), 491–503 (1992).

#150680 - $15.00 USD Received 7 Jul 2011; revised 19 Aug 2011; accepted 5 Sep 2011; published 8 Sep 2011

12. A. Mandelis, N. Baddour, Y. Cai, and R. G. Walmsley, "Laser-induced photothermoacoustic pressure-wave pulses in a polystyrene well and water system used for photomechanical drug delivery," J. Opt. Soc. Am. B **22**(5), 1024–1036 (2005).
13. S. Boonsang and R. J. Dewhurst, "Pulsed photoacoustic signal characterization incorporating near- and far-field diffraction effects," Meas. Sci. Technol. **16**(4), 885–899 (2005).
14. A. Mandelis, Y. C. Teng, and B. S. H. Royce, "Phase measurements in the frequency domain photoacoustic spectroscopy of solids," J. Appl. Phys. **50**(11), 7138–7146 (1979).
15. X. Chen, K. Q. Schwarz, and K. J. Parker, "Acoustic coupling from a focused transducer to a flat plate and back to the transducer," J. Acoust. Soc. Am. **95**(6), 3049–3054 (1994).
16. X. Chen, D. Phillips, K. Q. Schwarz, J. G. Mottley, and K. J. Parker, "The measurement of backscatter coefficient from a broadband pulse-echo system: a new formulation," IEEE Trans. Ultrason. Ferroelectr. Freq. Control **44**(2), 515–525 (1997).
17. J. E. Mark, *Polymer Data Handbook*, 2nd ed. (Oxford University Press, 2009).
18. H. Tohmyoh, T. Imaizumi, and M. Saka, "Acoustic resonant spectroscopy for characterization of thin polymer films," Rev. Sci. Instrum. **77**(10), 104901 (2006).
19. P. K. Wong, P. C. W. Fung, and H. L. Tam, "Low thermal diffusivity measurements of thin films using mirage technique," J. Appl. Phys. **84**(12), 6623–6627 (1998).
20. G. J. Diebold, "Theory of thin layer photoacoustic cells for determination of volume changes in solution," J. Phys. Chem. B **102**(27), 5404–5408 (1998).
21. F. A. Schaberle, R. M. D. Nunes, M. Barroso, C. Serpa, and L. G. Arnaut, "Analytical solution for time-resolved photoacoustic calorimetry data and applications to two typical photoreactions," Photochem. Photobiol. Sci. **9**(6), 812–822 (2010).
22. T. Autrey, N. S. Foster, K. Klepzig, J. E. Amonette, and J. L. Daschbach, "A new angle into time-resolved photoacoustic spectroscopy: A layered prism cell increases experimental flexibility," Rev. Sci. Instrum. **69**(6), 2246–2258 (1998).
23. F. L. Lizzi, M. Greenebaum, E. J. Feleppa, M. Elbaum, and D. J. Coleman, "Theoretical framework for spectrum analysis in ultrasonic tissue characterization," J. Acoust. Soc. Am. **73**(4), 1366–1373 (1983).
24. M. Y. Berezin, L. Hyeran, W. Akers, K. Guo, R. J. Goiffon, A. Almutairi, J. M. J. Frechet, and S. Achilefu, "Engineering NIR dyes for fluorescent lifetime contrast," in *Annual International Conference of the IEEE Engineering in Medicine and Biology Society, 2009. EMBC 2009* (2009), pp. 114–117.
25. S. I. Prajapati, C. O. Martinez, A. N. Bahadur, I. Q. Wu, W. Zheng, J. D. Lechleiter, L. M. McManus, G. B. Chisholm, J. E. Michalek, P. K. Shireman, and C. Keller, "Near-infrared imaging of injured tissue in living subjects using IR-820," Mol. Imaging **8**(1), 45–54 (2009).
26. A. Masotti, P. Vicennati, F. Boschi, L. Calderan, A. Sbarbati, and G. Ortaggi, "A novel near-infrared indocyanine dye-polyethylenimine conjugate allows DNA delivery imaging in vivo," Bioconjug. Chem. **19**(5), 983–987 (2008).
27. S. Telenkov and A. Mandelis, "Signal-to-noise analysis of biomedical photoacoustic measurements in time and frequency domains," Rev. Sci. Instrum. **81**(12), 124901 (2010).
28. G. A. Holzapfel, G. Sommer, C. T. Gasser, and P. Regitnig, "Determination of layer-specific mechanical properties of human coronary arteries with nonatherosclerotic intimal thickening and related constitutive modeling," Am. J. Physiol. Heart Circ. Physiol. **289**(5), H2048–H2058 (2005).
29. S. A. Prahl, I. A. Vitkin, U. Bruggemann, B. C. Wilson, and R. R. Anderson, "Determination of optical properties of turbid media using pulsed photothermal radiometry," Phys. Med. Biol. **37**(6), 1203–1217 (1992).
30. L. Nicolaides, C. Feng, A. Mandelis, and S. H. Abrams, "Quantitative dental measurements by use of simultaneous frequency-domain laser infrared photothermal radiometry and luminescence," Appl. Opt. **41**(4), 768–777 (2002).
31. E. Delaey, F. van Laar, D. De Vos, A. Kamuhabwa, P. Jacobs, and P. de Witte, "A comparative study of the photosensitizing characteristics of some cyanine dyes," J. Photochem. Photobiol. B **55**(1), 27–36 (2000).
32. M. Y. Berezin, H. Lee, W. Akers, and S. Achilefu, "Near infrared dyes as lifetime solvatochromic probes for micropolarity measurements of biological systems," Biophys. J. **93**(8), 2892–2899 (2007).
33. S. Ashkenazi, "Photoacoustic lifetime imaging of dissolved oxygen using methylene blue," J. Biomed. Opt. **15**(4), 040501 (2010).
34. B. Fückel, D. A. Roberts, Y. Y. Cheng, R. G. C. R. Clady, R. B. Piper, N. Ekins-Daukes, M. J. Crossley, and T. W. Schmidt, "Singlet oxygen mediated photochemical upconversion of NIR light," J. Phys. Chem. Lett. **2**(9), 966–971 (2011).
35. C. Franco and J. Olmsted III, "Photochemical determination of the solubility of oxygen in various media," Talanta **37**(9), 905–909 (1990).
36. T. R. Rettich, R. Battino, and E. Wilhelm, "Solubility of gases in liquids. 22. High-precision determination of Henry's law constants of oxygen in liquid water from T = 274 K toT = 328 K," J. Chem. Thermodyn. **32**(9), 1145–1156 (2000).
37. O. Abimbola and N. Tebello, "Solvent effects on the photophysicochemical properties of tetra (tert-butylphenoxy) phthalocyaninato zinc (II)," Acta Phys. Chim. Sin **27**(5), 1045-1052 (2011).
38. H. Gratz, A. Penzkofer, C. Abels, R. M. Szeimies, M. Landthaler, and W. Bäumler, "Photo-isomerisation, triplet formation, and photo-degradation dynamics of indocyanine green solutions," J. Photochem. Photobiol. Chem. **128**(1-3), 101–109 (1999).
39. H. Tian, "The influence on the triplet state in antenna rhodamine dyes of intramolecular energy transfer and charge transfer," J. Photochem. Photobiol. Chem. **91**(2), 125–130 (1995).

#150680 - $15.00 USD Received 7 Jul 2011; revised 19 Aug 2011; accepted 5 Sep 2011; published 8 Sep 2011

40. S. Murphy, B. Sauerwein, H. G. Drickamer, and G. B. Schuster, "Spectroscopy of cyanine dyes in fluid solution at atmospheric and high-pressure—The effect of viscosity on nonradiative processes," J. Phys. Chem. **98**(51), 13476–13480 (1994).
41. R. G. Kolkman, W. Steenbergen, and T. G. van Leeuwen, "Reflection mode photoacoustic measurement of speed of sound," Opt. Express **15**(6), 3291–3300 (2007).

1. Introduction

An excited molecule can return to its ground state through different pathways. Some of these pathways may include radiative transitions, which result in emission of photons and are called fluorescence or phosphorescence. The other transitions occur without emission of photon and are known as non-radiative transitions. In the modern medicine, different optical techniques, such as fluorescence lifetime (FL) measurement [1], are used to assess lifetime of a biomarker in an excited state. This type of assessment provides quantitative information about microenvironment in which molecules of the biomarker is situated. Measuring the excited state lifetime of a biomarker has applications like detection of brain tumors [2], diagnosis of blood pathologies [3], monitoring of microvessel oxygenation [4], and study of DNA dynamics [5]. Medical fluorescence imaging techniques, however suffer from loss of spatial information due to strong scattering of light in turbid media like tissue. Therefore developing other methods for assessment of the excited state lifetime besides fluorescence measurements is required to overcome such difficulties. In many instances non-radiative transitions either alone or in competition with fluorescence relaxation are responsible for the decay of molecules from an excited state to the ground state. Therefore study of non-radiative transitions also can provide information about relaxation dynamics of the excited state, which is affected by environmental properties. Recent studies have shown that measurement of the non-radiative relaxation time can provide a new source of contrast mechanism in photoacoustic imaging technique [6]. The non-radiative transitions are mainly characterized by heat generation and can be studied through produced thermal effects.

Recently two different methods were proposed to assess non-radiative relaxation of excited state for biological chromophore or exogenous biomarkers [7,8]. Both of these methods exploited pulsed photoacoustic (PA) probing which relies on the detection of transient pressure induced in a sample after the sample is irradiated by short laser pulses. In one of these works, saturation of the optical absorption at high fluences of laser light was used to measure non-radiative relaxation of biological chromophores and other fluorophores [7]. This method allowed to measure picoseconds non-radiative relaxation of molecules from singlet excited state to the ground state. The other technique exploited a double-pulse illumination method and enabled measurement of slower non-radiative relaxations from a triplet state to the ground state (timescales of microsecond) [8]. Pulsed photoacoustic detection requires relatively complex and more expensive lasers, suffers from laser jitter noise and has a limited dynamic range of broad band detection [9,10].

To overcome these disadvantages, we investigated the usability of intensity-modulated continuous-wave (CW) photoacoustic detection for measuring non-radiative relaxation time of macromolecules. In this method, an intensity-modulated CW light source promoted the molecules of chromophore in a sample to their excited state. The excited molecules can relax to the ground state either directly from this excited singlet state or after transition to excited triplet state which has longer lifetime compared to the excited singlet state. Upon returning to their ground state through non-radiative transitions from either of the aforementioned excited states, these molecules release heat and cause thermoelastic expansion of the target which can be detected as a CW photoacoustic signal. In CW photoacoustic detection, dependence of both amplitude and phase of the generated PA signal to the modulation frequency of exciting light have been used to assess non-radiative relaxation times of samples [11].

One drawback of CW photoacoustic technique is limited intensities of light allowed to be used in this method for medical purposes. For this reason, medical applications of CW photoacoustic detection are more sensitive to the thermal and other environmental noises compared to pulsed PA techniques. In this work we opted to use a tone-burst modulated light from a laser diode. Using high intensity laser diodes which are modulated with low duty cycle

#150680 - $15.00 USD Received 7 Jul 2011; revised 19 Aug 2011; accepted 5 Sep 2011; published 8 Sep 2011

tone bursts can produce relatively stronger PA signals while keeping biological sample from exposure to high energies of laser light. Another advantage of using a tone-burst modulation scheme is that a time resolved investigation of the resulting PA signal can provide information about sample characteristics along its depth. Due to available frequencies of light modulation and frequency response of the used ultrasound transducer, the current experiments allow measurement of slower non-radiative relaxations of molecules from their excited triplet states. A mathematical model previously developed by other group of researchers [10,12] was extended in this work to include the role of a finite value of non-radiative relaxation time in generation of laser-induced PA signal. Then three-dimensional effects caused by finite size of heated area on the target were added to the model through introduction of diffraction effects [12,13]. Experiments were performed on samples with fast non-radiative relaxations and the results were used to obtain their optical absorption coefficients. These values measured by photoacoustic technique were compared with results of optical spectroscopy to evaluate the model when non-radiative relaxations play no role in the PA signal. Then by using solutions of a NIR fluorescent dye in two different solvents, the effect of viscosity on non-radiative relaxation of excited dye molecules were verified.

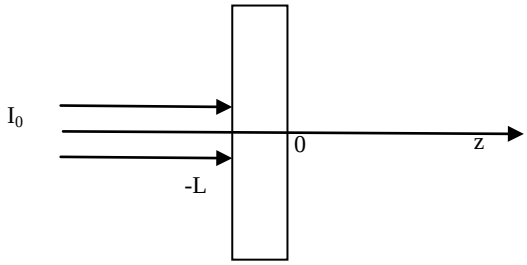

Fig. 1. Geometry used for formulating model of frequency dependent PA signal from a laser target illuminated by CW laser beam.

2. Theory

We used a mathematical model that describes the generation of PA signals from a plane target immersed in a liquid in a forward detection mode. Figure 1 shows the corresponding geometry used for this mathematical analysis. A light beam with incident intensity of I_0 illuminates the target. The two surrounding layers in the left and right sides of the target are considered semi-finite and extended in regions $-\infty < z \le -L$, $0 \le z < \infty$. The Fourier transform of the heat conduction equation for the angular modulation frequency of ω in the target layer can be written as a thermal-wave equation in form of

$$\frac{\partial^2}{\partial z^2}\theta(z,\omega) - \left(\frac{i\omega}{\alpha_t}\right)\theta_t(z,\omega) = -\frac{1}{\lambda_t}H(z,\omega), \tag{1}$$

where θ_t is the temperature rise in the target above ambient temperature, α_t and λ_t are, respectively, the thermal diffusivity and conductivity of the target. The source term in Eq. (1) is the Fourier transform of the induced heat in the target. For a periodically modulated laser beam with angular modulation frequency, the source term is given by

$$H(z,\omega) = \mu_a I_0 e^{-\mu_a(L+z)+i\omega t}. \tag{2}$$

This equation gives the generated heat in the target when it is caused by instantaneous non-radiative relaxation of molecules from their excited state to the ground state. In the case of samples with a finite non-radiative relaxation time τ, the source term in Eq. (1) will be in the form of [14]

$$H(z,\omega) = \frac{\mu_a I_0}{(1+i\omega\tau)} e^{-\mu_a(L+z)+i\omega t}. \tag{3}$$

#150680 - $15.00 USD Received 7 Jul 2011; revised 19 Aug 2011; accepted 5 Sep 2011; published 8 Sep 2011

Also, an equation in the form of

$$\frac{\partial^2}{\partial z^2}\theta_f(z,\omega)-\left(\frac{i\omega}{\alpha_f}\right)\theta_f(z,\omega)=0,\quad -\infty<z\le -L,\ 0\le z<\infty, \tag{4}$$

which is similar to Eq. (1) but does not have the heat source term, expresses the heat conduction inside fluid layers surrounding the sample. In this equation θ_f and α_f are respectively the temperature rise and the thermal diffusivity of the fluid. The solution of Eqs. (1) and (4) can be found using the thermal boundary conditions, which require

$$\theta_f(-L,\omega)=\theta_t(-L,\omega),\quad \lambda_t\frac{\partial}{\partial z}\theta_t=\lambda_f\frac{\partial}{\partial z}\theta_f\Big|_{z=-L}, \tag{5}$$

in which λ_f is thermal conductivity of the surrounding fluid. The thermoelastic expansion of the target is dealt with by introducing a displacement potential $\phi_t(z,\omega)$, which is related to the displacement vector $U_t(z,\omega)$, as

$$U_t(z,\omega)=\frac{\partial}{\partial z}\phi_t(z,\omega). \tag{6}$$

Then the Helmholtz equation for the displacement potential in the target can be written as

$$\frac{\partial^2}{\partial z^2}\phi_t(z,\omega)+k_t^2\phi_t(z,\omega)=\left(\frac{K_t\beta_t}{\rho_t c_t^2}\right)\theta_t(z,\omega), \tag{7}$$

where $k_t = \omega/c_t$ is the acoustic wave number in the target layer. Here c_t is speed of sound in the target, ρ_t, target's density, K_t, its bulk modulus, and β_t is isobaric thermal expansion coefficient of the target. Similarly the liquid motion can be described using a scalar potential of the velocity field ψ_{fi} which is related to the velocity as $v(z,\omega)=\partial/\partial z\,\psi_{fi}$. Here the subscript i = 1, 2 is to denote fluid layers in the left and right side of the target respectively. The motion of liquid because of the PA wave can be written as a wave equation:

$$\frac{\partial^2}{\partial z^2}\psi_{fi}(z,\omega)+k_f^2\psi_{fi}(z,\omega)=0, \tag{8}$$

where $k_f = \omega/c_f$ is the wave number of the acoustic wave in the fluid and speed of sound in it is denoted by c_f. The pressure fluctuation in the fluid is related to the velocity potential, ψ_{fi}, through

$$P(z,\omega)=-i\omega\rho_f\psi_{fi}(z,\omega). \tag{9}$$

The frequency domain pressure wave in fluid at the illuminated side of the target which is given by $P(z,\omega)=-i\omega\, C_1(\omega)e^{-ik_f(z+L)}$ is found in Ref. [10]. Relevant to our experiments, we obtain the frequency domain pressure wave at the back side of the target, as

$$\begin{aligned}P(\omega)=&\frac{\mu_a I_0 K_t\beta_t\rho_f c_f}{\lambda_t(1+i\omega\tau)\left(\sigma_t^2+k_t^2\right)\left(\sigma_t^2-\mu_a^2\right)\left[\left(\rho_t c_t+\rho_f c_f\right)^2 e^{ik_tL}-\left(\rho_t c_t-\rho_f c_f\right)^2 e^{-ik_tL}\right]}\\
&\times\Big\{\left(\rho_t c_t+\rho_f c_f\right)\left(\mu_a^2-k_t^2-\sigma_t^2+ik_t\mu_a\right)e^{(ik_t-\mu_a)L}+\left(\rho_t c_t-\rho_f c_f\right)\left(\mu_a^2-k_t^2-\sigma_t^2-ik_t\mu_a\right)e^{(ik_t+\mu_a)L}\\
&+\left(\rho_t c_t-\rho_f c_f\right)\left(k_t+i\sigma_t\right)k_t b_{tf}e^{-(ik_t+\sigma_t)L}+\left(\rho_t c_t+\rho_f c_f\right)\left(k_t-i\sigma_t\right)k_t b_{tf}e^{(ik_t-\sigma_t)L}\\
&+2\left[\omega k_t\rho_t(b_{tf}-1)+\rho_t c_t(\mu_a^2-\sigma_t^2)-ik_t\rho_f c_f(\mu_a+b_{tf}\sigma_t)\right]\Big\}e^{-ik_f z},\end{aligned} \tag{10}$$

#150680 - $15.00 USD Received 7 Jul 2011; revised 19 Aug 2011; accepted 5 Sep 2011; published 8 Sep 2011

where

$$b_{tf} = \frac{\left(\lambda_t \mu_a + \lambda_f \sigma_f\right)}{\left(\lambda_f \sigma_f + \lambda_t \sigma_t\right)}, \tag{11}$$

$$\sigma_t^2 = i\omega/\alpha_t, \quad \sigma_f^2 = i\omega/\alpha_f. \tag{12}$$

By using Eq. (10) and knowing the physical parameters of the target and the surrounding fluid (i.e. sound speed, optical absorption coefficient, thermal conductivity and diffusivity, bulk modulus and volumetric expansion coefficient), one can determine the non-radiative relaxation time of the target from dependence of the PA signal to the modulation frequency of the CW exciting light beam.

By introducing diffraction effects of the acoustic wave in the model, it is possible to account for finite size of photoacoustic source [12]. Since the target is placed in focal point of the laser, and the diameter of the laser spot is negligible compared to aperture of the transducer, diffraction of PA signal originated from the target and detected by a focused transducer can be expressed as [15,16]

$$D(\omega) = -\left\{1 - e^{iG_p}\left[J_0(G_p) - iJ_1(G_p)\right]\right\}, \tag{13}$$

where r_0 is geometrical focal length, and the focusing factor of the transducer is defined as $G_p \equiv ka^2/2r_0$, in which a is aperture of the transducer. J_0 and J_1 denote respectively Bessel functions of order zero and one. The diffraction correction factor $D(\omega)$ as formulated by Eq. (13) can be inserted into Eq. (10) in the form of a spectrum transfer function to take into account diffraction effects, which arise from the three-dimensional nature of the problem. However in the range of frequencies used in the present work, modifications on the PA signal due to this effect are small.

Although the model presented here is used for calculating forward laser-induced PA pressure waves from a plane target, but a similar approach can be used to develop a similar model for the case of signals generated in a more general geometry and in backward detection mode.

Table 1. Physical properties used in the mathematical model of frequency domain photoacoustic effect

Material	ρ (kg/m^3)	c (m/s)	λ (W/mK)	α (m^2/s)	β (K^{-1})	Ref.
water	998	1480	0.61	0.1×10^{-6}	2.1×10^{-4}	[10]
silicone	1045	1030	0.16	0.098×10^{-6} (1)	6.9×10^{-4}	[17]
PVC film	1350	1750	0.15	0.08×10^{-6} (2)		[18]

(1)Calculated by $\alpha = \lambda/\rho C_p$, where C_p is the specific heat.

(2)Ref. [19].

To demonstrate the effect of finite non-radiative relaxation time on frequency dependent amplitude of the PA signal, theoretical simulations were carried out. Physical properties of an optically absorbent polyvinyl chloride film as they are listed in Table 1 are used for those of the target. The thickness of the target was assumed to be 1 mm and its optical absorption coefficient 100 cm^{-1}. The fluid surrounding the target was considered to be water. A wide range of modulation frequencies were used and diffraction effects were ignored. Normalized amplitudes of PA signal versus modulation frequency of the light for different values of non-radiative relaxation times were calculated using the mathematical model developed in this section. Results of these calculations in log-log scale are shown in Fig. 2 and agree well with results of frequency domain photoacoustic spectroscopy in a cell [14]. Similar to cell-based

#150680 - $15.00 USD Received 7 Jul 2011; revised 19 Aug 2011; accepted 5 Sep 2011; published 8 Sep 2011

photoacoustic spectroscopy, one of predictions of the theoretical model presented here is that for samples with very fast (instantaneous) non-radiative relaxation ($\tau = 0$), the amplitude of the PA signal with increase of the modulation frequency decay following a dependency of ω^{-1} to the modulation frequency. The finite non-radiative relaxation time ($\tau > 0$) causes breakage of the curve at high frequencies and approach to logarithmic slopes higher than that for the instantaneous curve.

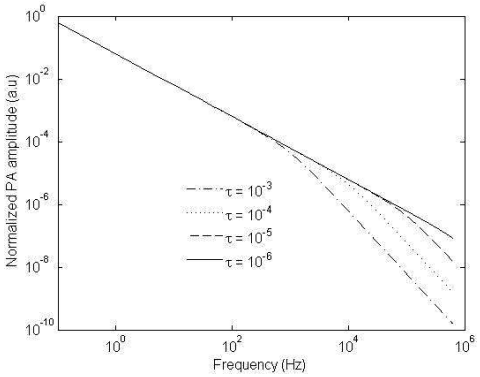

Fig. 2. Prediction of the theoretical model developed in this work on frequency dependence of the PA amplitude for targets with different non-radiative relaxation times. Physical properties of the target are those of PVC film listed in Table 1. The thickness of target is assumed to be 1 mm and its optical absorption coefficient is $\mu_a = 100$ cm^{-1}. The induced photoacoustic pressure is detected 2.54 cm far from the target surface and on the *z*-axis.

The model predicts that for detecting shorter non-radiative relaxation times, higher frequencies of the modulation are needed. The conclusion is in agreement with the assessment that in pulsed photoacoustic experiments for measuring short lifetime, using laser pulse widths that are shorter than required lifetime measurement resolution is necessary [8]. Direct modulation of intensity of CW light to higher frequency (until few hundred megahertz) is easier and cheaper than that of pulsed picosecond laser sources.

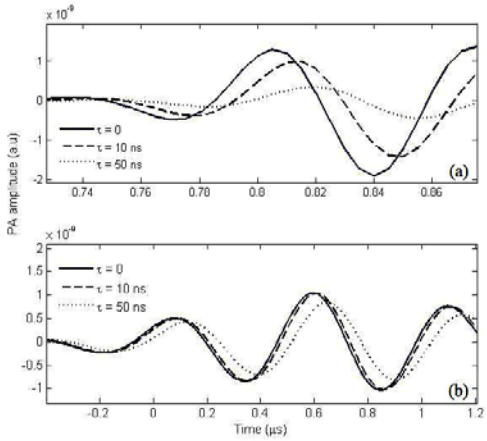

Fig. 3. Time domain simulation of the PA signal for a configuration commonly used in time-resolved calorimetry for ultrasound transducer with central frequency of (a) 15 MHz, (b) 2.25 MHz.

Since the geometry of our model is similar to the geometry often used in time-resolved photoacoustic calorimetry [20], the model developed here is also used to simulate results of such experiments. The geometry dependent PA transfer function given by Eq. (10) must be

#150680 - $15.00 USD Received 7 Jul 2011; revised 19 Aug 2011; accepted 5 Sep 2011; published 8 Sep 2011

multiplied by frequency response of the ultrasound transducer, which is used to detect the PA signal. Since in time-resolved photoacoustic calorimetry, laser pulses usually have short duration, hence their spectral profile is much broader than transducer bandwidths. Therefore, compared to frequency response of the transducer, frequency response of the laser pulse can be neglected. The time-dependent PA signal can be calculated by taking inverse Fourier transform of the resulting frequency domain pressure function. The results of such simulation using our model and for different values of non-radiative relaxation times are shown in Fig. 3 for two transducers with central frequencies of 2.25 MHz and 15 MHz. These results are in agreement with results of time-resolved PA calorimetry [21,22].

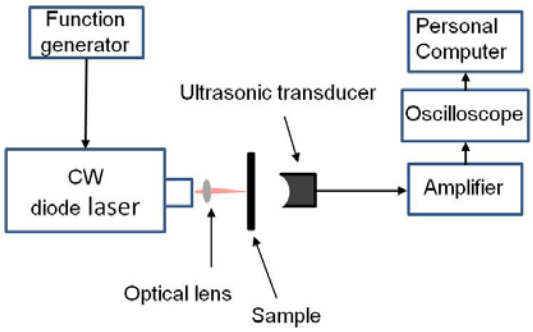

Fig. 4. Block diagram of experimental setup used in CW intensity-modulated laser-induced PA measurements.

3. Experiment

To test this theoretical model for extraction of non-radiative relaxation time from PA signals, measurements were carried out using an experimental configuration shown in Fig. 4. The PA signals were induced in targets by tone-burst intensity modulated beams from a diode laser (L808P200, ThorLabs, Newton, NJ; power: 200 mW; wavelength: 808 nm). The diode laser was driven by a laser diode current controller (LDC220, ThorLabs, Newton, NJ) and its power was modulated in burst mode with 5 cycles at different modulation frequencies. A modulation depth of 50% was used by applying 10 V_{pp} electric signal from a function generator (33250A, Agilent, Santa Clara, CA) to the laser bias through an input with 50 Ω impedance. The repetition rate of the burst signal was set to be 1 kHz. The transmitted light directly illuminated the target at focal point of the laser diode in a distance of 5 mm. The focalized spot was secured to be aligned on the axis of the transducer. The output power of laser diode for different modulation frequencies was measured and has been found that it stays constant in the range of modulation frequencies of the current work. A high curvature focused ultrasonic transducer (V315, Olympus NDT, Waltham, MA; 1 inch focus length, 10 MHz) was used to detect the PA signals from the target. The resulting signal was amplified by an amplifier (5072PR, Olympus, Waltham, MA) and registered on an oscilloscope (Tektronix DPO3034, Tektronix Inc, Beaverton, OR, 80 MHz) to be processed later. Frequency response of the transducer was found by measuring the amplitude of reflection for tone-burst signals at different modulation frequencies from a ¼ inch thick borosilicate glass (McMaster-Carr, Chicago, IL) placed at the focal point of the transducer [23].

Two samples were prepared by mixing black ink from permanent marker with commercially available 1-part silicone elastomer. The mixture was left in the room temperature to cure. The thickness of the resulting silicone phantoms was measured by a digital caliper (Fred V. Fowler Co., Inc., Newton, MA) and was determined to be 1.57 ± 0.13 mm (mean ± standard deviation) for the target with a lower absorption and 0.96 ± 0.1 mm for the target with higher absorption coefficient. By using an optical spectrometer (Thorlabs SP2-USB, wavelength 500 to 1000 nm, Thorlabs, Newton, NJ) the optical densities (*OD*) of the two samples were measured in 5 different points. Knowing the mean thickness of the

#150680 - $15.00 USD Received 7 Jul 2011; revised 19 Aug 2011; accepted 5 Sep 2011; published 8 Sep 2011

phantoms and by using the Beer-Lambert law, $\mu_a = (2.303 \times OD)/L$, the optical absorption coefficients of the two targets at the wavelength of 808 nm were determined to be 2235 ± 412 m^{-1} and 7130 ± 955 m^{-1} (mean ± standard deviation). The uncertainties on the measured optical absorption coefficients are due to local inhomogeneities in resulting phantoms and also relatively considerable variation of thickness in different locations of the sample.

To demonstrate performance of the proposed technique and validate the developed mathematical model for estimating non-radiative relaxation time, measurements were performed on solutions of a near infrared (NIR) dye in two different solvents. IR820 (Sigma-Aldrich, St. Louis, MO) is a chlorinated heptamethine indocyanine dye with fluorescence lifetime of 0.13 ns in water and maximum optical absorption around 820 nm [24]. It is used for imaging of injured tissue in living subjects [25] and non-invasive monitoring of DNA delivery by using its conjugate with Polyethylenimine (PEI) [26]. Its optical absorption in near infrared with a peak absorption around 820 nm places IR-820 amongst the best candidates for being used in the current experimental setup which is using a diode laser with wavelength of 808 nm. Two solutions of 624 μM and 849 μM of IR820 dye respectively in deionized water and dimethyl sulfoxide (DMSO) were prepared. The dye solutions were then purred in space between two thin layers of optically clear polyvinyl chloride (PVC) films which were water sealed by sealing glue. The thickness of each film was determined to be 140 μm.

The amplitude of the PA signals from different targets for different modulation frequencies of laser light were obtained by using the cross-correlation operation, also known as matched filtering on the detected ultrasound signal with the reference signal of the intensity-modulated light [27]. Examples of laser-induced tone-burst PA signal from optically absorbant silicone phantom and resulting signals after applying the matched filtering with the reference signal are shown in Fig. 5. Finally these results were normalized to the frequency response of the transducer.

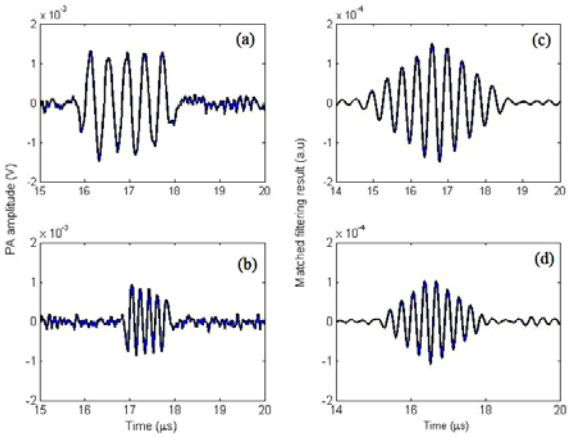

Fig. 5. Photoacoustic signals induced in phantom #1 made of silicone elastomer mixed with black ink after its illumination by tone-burst modulated laser light at 808 nm (a,b) and the result of matched filtering by the reference signal on them (c,d) for light modulation frequencies of 2.25 MHz (a,c) and 5.25 MHz. (b,d).

4. Results and discussion

The theoretical model presented here was used to fit experimentally obtained frequency dependent PA amplitudes, and to obtain optical absorption coefficient and non-radiative relaxation time of the targets. Similar to previous works by other group [10] we found that the fitting procedure is not very sensitive to exact values of volumetric thermal expansion coefficient, β_s, thermal diffusivity, $\alpha_{s,f}$, thermal conductivity, $\lambda_{s,f}$ and bulk modulus, K_s. In

#150680 - $15.00 USD Received 7 Jul 2011; revised 19 Aug 2011; accepted 5 Sep 2011; published 8 Sep 2011

contrast, the values of sound speed, sample thickness, and its optical absorption coefficient were important parameters for fitting. For fitting procedure the known values of sound speed, thermal diffusivity, thermal conductivity, bulk modulus, thermal expansion coefficient and density from literature were used, which are listed in Table 1. The remaining parameters was found by using a nonlinear least square algorithm lsqnonlin in MATLAB® software (The Mathworks, Natick, MA) to minimize sum of squared residuals between experimental data and numerical results of Eq. (10). By changing parameters of the model in a reasonable range of values, several fitting results to the experimental data were found. The best fit among these fitting results was selected by looking for the smallest root-square-mean-error (RMSE) [28] as a measure for the "goodness of fit". This procedure is similar to global fitting procedures previously employed for determining optical parameters of turbid media from pulsed or frequency domain photothermal radiometries [29,30].

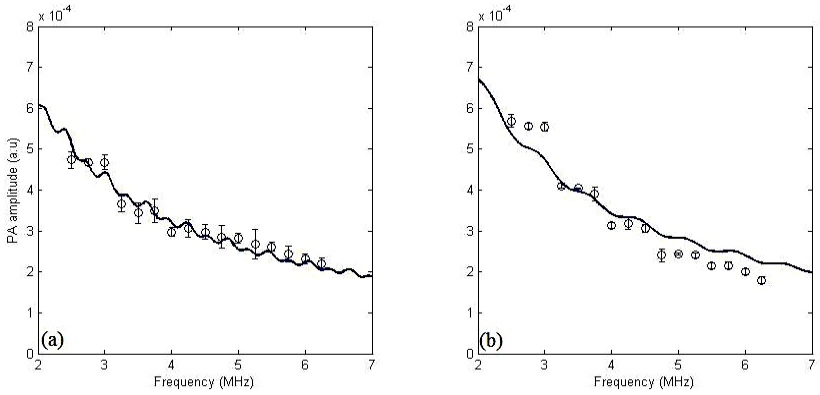

Fig. 6. Experimental and best-fit for PA amplitude versus laser intensity modulation frequency from the silicone phantoms #1 (a) and the phantom #2 (b). The best fits for the phantoms 1 and 2 are found for μ_a = 2300 m^{-1} and μ_a = 7100 m^{-1} respectively. The physical properties used for fitting are listed in Table 1.

The experimental and best-fitted frequency dependence of PA amplitude from two absorbing phantoms of silicone elastomer are presented in Fig. 6. Logarithmic slopes of the frequency dependence PA amplitude for the two silicone phantoms are −0.84 and −1.31, respectively, for the phantom with lower optical absorption and that with a higher optical absorption. These values are not equal to the logarithmic slope of −1, which is characteristic of a sample with instantaneous non-radiative relaxation time. This difference can be attributed to oscillatory behavior originated from creation of standing acoustic waves between two surfaces of the target [10]. This oscillatory behavior is to a better extend reflected by fitting, especially in the case of phantom with lower optical absorption, through the more complete mathematical model developed in Section 2. Physical properties of phantoms obtained by fitting the experimental data with the model are listed in Table 2 and are compared with measurements of the optical absorption coefficient of phantoms using a spectrometer. The discrepancies between experimental and theoretical values obtained from these results are due to sensitivity of the CW photoacoustic measurements to thermal noise and mechanical vibrations in the experimental environment [27].

One limiting factor in our experiments is the modulation depth of laser intensity (around 50%). Increasing the modulation depth and using higher intensities of the laser light are required for increasing the PA signal and reducing the limiting factor of environmental noise. Amplitude of the PA signal drops rapidly to the level of noise with the increase of the light modulation frequencies. Therefore using highly sensitive broadband ultrasound transducers are desirable for measuring shorter non-radiative relaxation times by using high frequency modulation. Another possible reason for the observed differences between numerical results

#150680 - $15.00 USD Received 7 Jul 2011; revised 19 Aug 2011; accepted 5 Sep 2011; published 8 Sep 2011

Table 2. Obtained parameters through fitting the theoretical model with experimental PA data and their comparison with values measured by other methods

	Phantom #1		Phantom #2	
	PA measurement	direct measurement	PA measurement	direct measurement
μ_a (m^{-1})	2300	2235 ± 235 (mean ± SD)	7100	7130 ± 1131 (mean ± SD)
l (mm)	1.7	1.57 ± 0.13 (mean ± SD)	0.7	0.96 ± 0.1 (mean ± SD)
R^2	0.94		0.915	
RMSE	2×10^{-5}		3.86×10^{-5}	

and the experimental data can be the relatively high sensitivity of the model on the changes in sound speed. A more accurate determination of this parameter can eventually improve the outcome of the fitting. Regardless of these difficulties, the fitting procedure with PA signals provides an estimation of optical absorption coefficients for the two silicone phantom samples, which agree fairly well with measurements of this parameter by the spectroscometer. In the case of silicone phantoms, no noticeable improvement in fitting results was observed by introducing an appreciable non-zero value of non-radiative relaxation time.

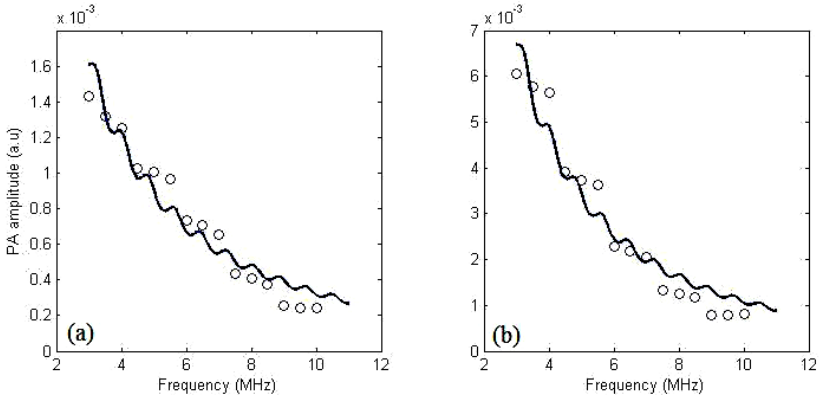

Fig. 7. Experimental and best-fit for PA amplitude versus laser intensity modulation frequency from solution of IR820 in two different solvents. (a) IR820 in water; the fitting parameters are $\mu_a = 9.15 \times 10^5$ m^{-1}, $\tau = 21.5$ ns (b) IR820 in DMSO; the fitting parameters are $\mu_a = 1 \times 10^6$ m^{-1}, $\tau = 3.29$ ns. The physical properties used for the target and the surrounding water are listed in Table 1.

Figure 7 shows measurement results and best-fitted frequency dependence of PA amplitude versus modulation frequency of laser light in the solution of IR820. The values of −1.62 and −1.93 are obtained for logarithmic slopes of the frequency dependence PA amplitude dissolved IR820 in water and DMSO, respectively. This shows that one can expect longer non-radiative relaxation times for solution of IR820 in DMSO. Knowing the molar absorption coefficient of IR820 in water [30] ($\varepsilon = 1466000$ cm^{-1} at $\lambda = 824$ in water) by considering the concentration of aqueous solution, which is 624 μM and for a conservative thickness of 1 mm, one finds an absorption coefficient of 9150 cm^{-1} for this solution. This value is not considered excessively high but it is close to the upper limit of resolvable absorption coefficient through PA measurements [10]. Since NIR dyes generally have poor solvatochromic properties [31,32], one can assume a similarly high absorption coefficient of dissolved IR820 in DMSO. The fitting with experimental data yields a best fit for non-radiative relaxation time of 21.5 ns and 33 ns for solutions of IR820 in water and DMSO respectively. The parameters of fit for these two samples are $R^2 = 0.941$, RMSE = 9.96×10^{-5} for the aqueous solution of IR820 and $R^2 = 0.949$, RMSE = 4.31×10^{-5} for dissolved IR820 in

#150680 - $15.00 USD Received 7 Jul 2011; revised 19 Aug 2011; accepted 5 Sep 2011; published 8 Sep 2011

DMSO. This slowly released heat in the dye solutions can be mainly attributed to non-radiative deactivation of triplet state [11,33]. Although in oxygen-free solutions, IR820 shows a low triplet quantum yield however its triplet yield increases in presence of oxygen [34]. At the same time, oxygen in solution can accelerate deactivation of the triplet state upon collisions [33]. Since solubility of oxygen in air-saturated DMSO, 0.33 mM [35], is higher than that for water [36], 0.28 mM, and because the two solutions are prepared in normal atmosphere without degassing, therefore it is reasonable to assume that concentration of oxygen in the prepared aqueous solution is not much higher than that in the solution of IR820 in DMSO.

Previous studies have shown that solutions of oxygenated IR820 exhibit a weak delayed fluorescence with decay times on the order of 100 ns [34]. This E-type delayed fluorescence is attributed to enhanced intersystem crossing in presence of dissolved oxygen [34]. It also has been shown that triplet lifetime increases with the increase in solvent viscosity [37]. Gratz *et al.* [38] have found that dwell time, which is a measure of efficiency for triplet-state accumulation, for indocyanine green sodium iodide (ICG-NaI), in N2-bubbled solutions of dye in DMSO is in the range of 35 ns while this value for solutions of this dye in N2-bubbled water is only 1.2 ns. A similar trend for lifetime of triplet state in solutions of different rhodamine dyes in two different solvents, ethanol and ethylene glycol, has been observed elsewhere [39]. Although complete explanation of dependence of non-radiative relaxation of dye molecules on viscosity of solvent needs more thorough insight on the photochemistry of this process, however, this dependence has already been shown [40]. In addition to previously mentioned factors such as high sensitivity to thermal and vibrational noise in environment, which affect the quality of fitting results, in the case of PA experiments with dye solutions there is also existence of two layers of PVC film between the target solution and the coupling fluid (water). Using an effective value for speed of sound [41] and an average value for density of the ensemble of the system can possibly improve the results of fitting.

5. Conclusion

A new method based on PA effect induced in a target by tone-burst intensity-modulated light from laser diode is investigated to assess non-radiative relaxation time of biological chromophores. A mathematical model is developed to incorporate the effect of a finite non-radiative relaxation time on the frequency dependence of PA amplitude. The results of this model by varying non-radiative relaxation time are compared against results of cell-based PA spectroscopy and a good agreement between these two have be found. Also it is shown that the model is capable of correctly predict time-domain behavior of the PA signals observed in time-resolved PA calorimetry experiments.

Experiments on samples with fast non-radiative relaxation times were performed. The results have shown that estimated optical absorption coefficients from resulting data are in agreement with measurements of the same parameter by optical spectroscopy. The CW PA measurements on solutions of the NIR dye, IR820 in two solvents water and DMSO by the proposed method resulted in two different values of non-radiative relaxation time. IR820 dissolved in DMSO resulted in a non-radiative relaxation time 1.5 times higher than that for the dye in water. This behavior is explained based on effect of solvent viscosity on lifetime of triplet state. The measurements have the potential to map excited state lifetime of a NIR dye and to obtain information about microenvironment surrounding its molecules in tissue. The advantage of using this method in NIR region of the light spectrum is that in this region, light penetrate deeper in the tissue compared to the ultraviolet or visible light. Also due to smaller scattering of NIR light in tissue compared to visible light, PA images with submillimeter lateral resolution can be achieved.

Acknowledgments

The authors would like to acknowledge financial support from NIH 1R03DA026987 and 1R21EB010184.

#150680 - $15.00 USD Received 7 Jul 2011; revised 19 Aug 2011; accepted 5 Sep 2011; published 8 Sep 2011